Supplemental Information for

Evaluation of SERS Substrates from Single-Molecule Statistics

Evan J. Kiefl[1], Robert F. Kiefl[2], Diego P. dos Santos[3], Alexandre G. Brolo[1,4]*

[1]*Department of Chemistry, University of Victoria, Victoria, V8P 5C2, Canada*

[2]*Department of Physics and Astronomy, University of British Columbia, V6T 1Z4, Canada*

[3]*Department of Physical Chemistry, Institute of Chemistry, University of Campinas, Campinas, São Paulo, CEP 13083-970, Brazil*

[4] *Center for Advanced Materials and Related Technologies (CAMTEC), University of Victoria, Victoria, BC, V8W 2Y2, Canada*

Corresponding author: agbrolo@uvic.ca

Review of single HS theory

When two spherical metallic NPs are irradiated with light (Figure S1), the resultant SERS enhancement factor F is distributed over the surface of each sphere such that the probability density function (pdf) of a randomly adsorbed molecule experiencing an enhancement F is given by a truncated Pareto distribution (TPD)[1]:

$$p(F) = \begin{cases} \dfrac{k}{F_m^{-k} - F_M^{-k}} F^{-(1+k)}; F_m < F < F_M, \\ 0 \text{ otherwise} \end{cases} \quad \text{(S1)}$$

where k is a measure of how fast F decays when moving away from the HS on the surface of the nanostructure, and F_m and F_M are the lower and upper bounds over which the distribution is defined. $k/\left(F_m^{-k} - F_M^{-k}\right)$ is the normalization factor of the pdf.

Herein we refer to F being distributed according to Eq. S1, however, one should keep in mind that SERS intensity (I) measurements are proportional to $F$and hence are also distributed according to Eq. S1, with $F \to I$, $F_m \to I_m$, and $F_M \to I_M$.

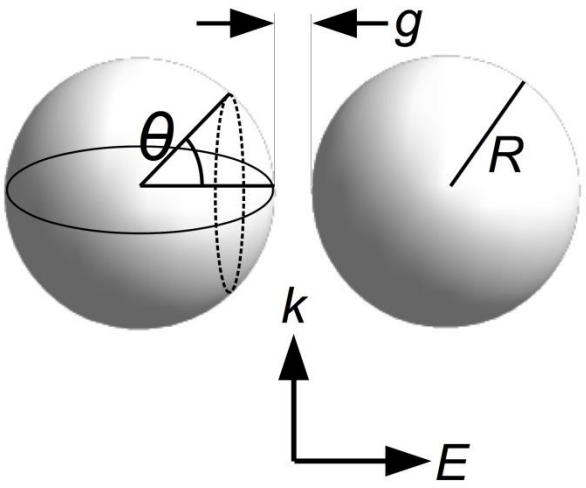

Figure S1: An idealized nanosphere dimer. The spheres, each of radius $\boldsymbol{R}$, are separated by an interparticle gap distance $\boldsymbol{g}$ and irradiated with a laser light of wavelength $\boldsymbol{\lambda}$, oriented such that the electric field $\boldsymbol{E}$ oscillates parallel to the dimer axis. $\boldsymbol{\theta}$ is a polar angle defining a circle on the sphere's surface (dashed line) and is oriented such that $\boldsymbol{\theta = 0}$ is along the dimer axis, *i.e.* at the center of the HS. Due to reflection symmetry, $\boldsymbol{\theta}$ can be defined on either sphere.

In view of the relationship between F and I, it is useful to consider F_m an instrumental parameter corresponding to the minimum F measurable by an instrument in a SM event. On the other hand, we define F_M to be the maximum F on the substrate (in SM experiments this does not approach the maximum detection limit of the instrument). F_M is, therefore, a physical parameter and is called the "strength of the HS", which occurs at $\theta = 0°$ in Figure S1.

The characteristic feature of a TPD is that when viewed on a log-log plot, $p(F)$ is a straight line. This was first observed over a large range of enhancements for a silver dimer substrate with 25 nm radii nanoparticles (NPs) separated by a gap distance of 2 nm and irradiated with a 448 nm wavelength radiation[2]. The results have been reproduced here with similar methods. Figure S2 shows $F(\theta)$, calculated in terms of the E^4-approximation[3] (Eq. S2, where E_{loc} and E_0 are the local and incident electric fields, respectively), and $p(F)$ for the system shown in Figure S1.

$$F = \left(\frac{E_{loc}}{E_0}\right)^4 \quad \text{(S2)}$$

The $p(F)$function is determined in a Monte Carlo-like procedure, in which it is generated a distribution of angles θ according to its probability distribution on the surface of a sphere p(θ)=(1/2) sin(θ) that describes the probability of finding a molecule at a given distance θ from the HS center. The values of F(θ) were then used to generate the distribution of F values ($p(F)$) on the surface of a sphere.

$F(\theta)$ describes the dependence of F along the surface of either sphere and $p(F)$ is the pdf for F values on either sphere. $p(F)$ is represented in log-log form, and thus the solid line (red) region in Figure 2 clearly shows the TPD behavior. The θ values from which these TPD-statistics are derived spans 0 - 36º (highlighted in red in Fig. 2). When F is less than ~5×10^4, multiple θ values lead to the same F, which is the cause of the rapid deviation from TPD behavior.

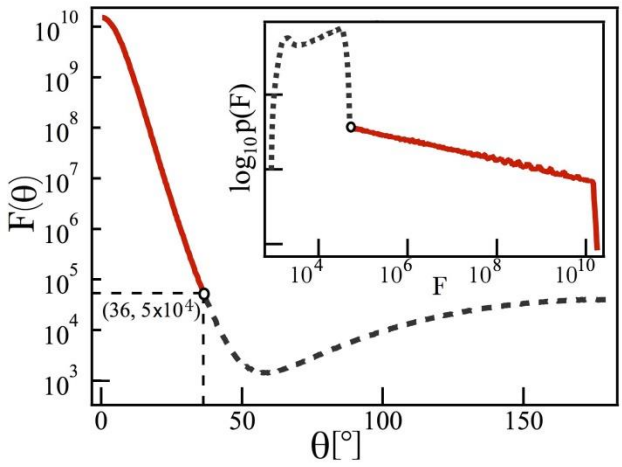

Figure S2: Distribution of enhancements for the scenario described in **Figure S1**. Silver nanosphere dimers (***R***=25nm, ***g***=2nm) irradiated with ***λ***=448nm laser light (in resonance with the dimer dipolar plasmon mode) are the parameters used for the simulation, although the results are qualitatively representative of all (***R***,***g***,***λ***) combinations which manifest strong HSs, an observation tested for gold and silver dimers in ref. 2. The ***F*** values were calculated 0.5 nm above the surface to reflect the finite size of adsorbing molecules. The inset shows $\boldsymbol{p}(\boldsymbol{F})$ represented in log-log form, where the TPD region (solid red line) spans over 5 orders of magnitude. This large range can be observed in the main figure (solid red line) to be the result of an incredibly rapid decay from the center of the HS. In both figures, the dashed black lines correspond to non-TPD enhancements and are insignificantly small in comparison.

An essential question with regards to the TPD-HS model is how well it recapitulates the statistics of SERS measurements. The exceptional degree of linearity in the log-log representation of $p(F)$ implies the model tightly converges to $p(F)$ at mid to high F values, but there is still non-TPD behavior (dashed black line) at low F values, when values of F are accessible from multiple theta values (and therefore multiple regions of the substrate). Also concerning is that only 10.2% of the surface area of the sphere obeys TPD-statistics, implying only a small fraction of adsorbed molecules obey TPD-statistics. Regardless, the percentage of the total average SERS signal produced by these TPD-obeying molecules is 98.98%. In practical terms, this means the HS is *fully* characterized by TPD statistics. A caveat to this observation is that the TPD region extends almost 6 orders of magnitude with respect to F, which might fall beyond the dynamic range of certain instruments. So from an experimental perspective, it is

more relevant to quantify how much of the total average signal originates from within the dynamic range. As long as this is close to 100%, the collected statistics accurately represent the statistics of the entire HS. For example, choosing $F_m = 1 \times 10^{7.9}$ as a hypothetical instrumental detection limit yields 98.9% of the signal, which is still the vast majority of the total signal, even though this hypothetical instrument detection range spans only 2 orders of magnitude in F.

Multiple hot-spot theory

In this section we develop a multiple HS model that incorporates the TPD nature of individual HSs. In particular, the model defines the probability density function that a molecule experiences an enhancement F, given that it adsorbed randomly onto a multi-HS substrate. We henceforth denote this pdf $g(F)$, the multi-HS equivalent of $p(F)$.

Suppose in an experiment one measures a SERS intensity signal, denoted F, from a substrate with Q HSs (notice that here we considered "SERS intensity" – a measured quantity – directly proportional to "enhancement factor" (F); therefore, we did not differentiated between them during the derivation). Let us define the latent variable Z, which informs which HS generated the signal F. For example, if $Z = q$, F was generated from the qth HS and; therefore, is distributed according to $p(F; k_q, F_{M,q})$ (Eq. S1), where k_q and $F_{M,q}$ are the TPD parameters of the qth HS. An assumption carried with the introduction of Z is that each HS is statistically independent from its neighbors, a requirement satisfied whenever HSs are sufficiently separated from one another. In general, this is easily satisfied given the intense localization of HSs. For example, in ref. 4 it can be observed visually that for a chain of nanoparticles, adsorption regions midway between two HSs exhibit enhancements over 5 orders of magnitude lower than the HS strengths, which can also be observed in our simulations (see Figure S10). Within this framework, $g(F)$ can be treated as a mixture distribution with Q subpopulations:

$$g(F) = \sum_{q=1}^{Q} w_q p\left(F; k_q, F_{M,q}\right). \tag{S3}$$

$p\left(F; k_q, F_{M,q}\right)$ is a TPD with parameters k_q and $F_{M,q}$ and is the pdf for the molecule adsorbed onto the qth HS. w_q is the probability that the molecule adsorbs onto the qth HS. Considering that it adsorbs randomly onto the surface of the substrate, w_q is just proportional to the surface area of the qth HS. Mathematically, $w_q = S_q / \sum_q^Q S_q$, where S_q is the surface area of the qth HS. S is defined as the adsorption area that exhibits enhancements greater than the instrumental detection limit F_m, and depends upon the parameters k and F_M. For example, a HS with large k will have a smaller S compared to one with smaller k but the same F_M.

Eq. S3 is useful in cases when there are a small number of HSs or when the characteristics of each HS are known. However, since the number of variables increases linearly with HS number, Eq. S3 is unsuitable for fitting to histograms generated from real systems, which possess a large number of HSs. To reduce the number of variables, we impose a continuum approximation on Eq. S3 by supposing each HS has parameters S, k, and F_{M} that are continuous random variables governed by a weighting factor $w(S, k, F_M)$. $w(S, k, F_M)$ is defined as the probability that a molecule adsorbs to a HS having surface area S, scaling parameter k, and strength F_M. Then, the continuous version of Eq. S3 is given by

$$g(F) = \iiint_{\Omega} w(S, k, F_M) p(F; k, F_M)\ \mathrm{d}S\mathrm{d}k\mathrm{d}F_M, \tag{S4}$$

where Ω is the integration space and $p(F; k, F_M)$ is given by Eq. S1. Note that even though S does not appear explicitly in $p(F; k, F_M)$, it is an implicit parameter because it depends upon k and F_m.

In order to use the model (Eq. S4) to infer substrate parameters, a parameterized form of the weighting factor $w(S, k, F_{\mathrm{M}})$ must be proposed. In the next section we simulate a substrate to both explore general characteristics of Eq. S4 and define a reasonable form of $w(S, k, F_{\mathrm{M}})$.

Simulated substrate

Enhancement distribution for multi-HS substrates

To better understand the influence of multiple HSs and the form of Eq. S3 and its continuum approximation (Eq. S4), we calculated $g(F)$ for a simulated substrate based on the archetypal silver nanosphere dimer system studied in ref. 2, whose results are presented in Figure S2. Instead of a single dimer, the substrate is modeled by a collection of 3500 independently behaving dimers with normally distributed radii and gap values ($\mu_R = 25$nm, $\sigma_R = 5$nm, $\mu_g = 2$nm, $\sigma_R = 0.5$nm). The variation in R and g is chosen to reflect the approximate experimental capabilities in producing uniform substrates. The system is irradiated with 448 nm light, which is the dipolar resonant wavelength of the mean geometry. For simplicity, each dimer axis is assumed to be parallel with the electric field; if they were randomly polarized, more variation in F_M would be observed. $F(\theta)$ and $p(F)$ were calculated for each HS, from which the parameters S, k, and F_M were extracted.

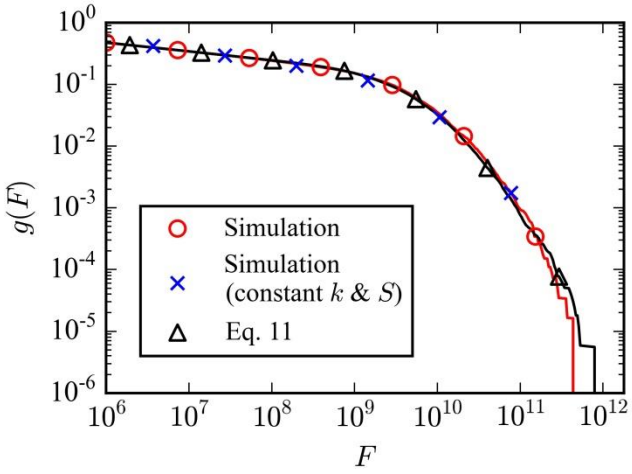

Figure S3: A compilation of $\boldsymbol{g(F)}$ curves. $\boldsymbol{g(F)}$ for the simulated substrate (red circles) was calculated via Eq. S2 and displays deviation from the power-law behavior seen in single dimer systems. Blue x's represent $\boldsymbol{g(F)}$ for the simulated substrate under the assumption that $\boldsymbol{S}$ and $\boldsymbol{k}$ are non-varying. The alikeness of these two curves (red circles and blue x's) indicates that deviation from power-law behavior is a result of the extreme variation observed in $\boldsymbol{F_M}$. Also shown is the least-squares fit of the simulated substrate (red circles) to Eq. S10 (black triangles). The fitted parameters are shown in Table I and the overall convergence of the fit validates the assumptions used to develop Eq. S11.

With knowledge of S, k, and F_M for each HS, $g(F)$ was calculated via Eq. S3 under the assumption of a hypothetical instrumental detection limit of $F_m = 1 \times 10^6$ (red circles in Figure S3). In log-log form, the curve exhibits a pseudo-linear region at low enhancements and a gradual bending at high enhancements. The deviation from power law behavior at large enhancements is the result of a large variation in F_M caused by a decreasing number of HSs contributing to the distribution at high enhancements, as was predicted in ref. 2.

2. Parameterization of the weighting factor

To determine an appropriate form of the weighting factor $w(S, k, F_M)$, we analyze how S, k, and F_M are distributed within the simulated substrate by calculating the marginal distributions $w_S(S)$, $w_k(k)$, and $w_{F_M}(F_M)$, *i.e.* normalized histograms of the parameters S, k, and F_M (Figure S4).

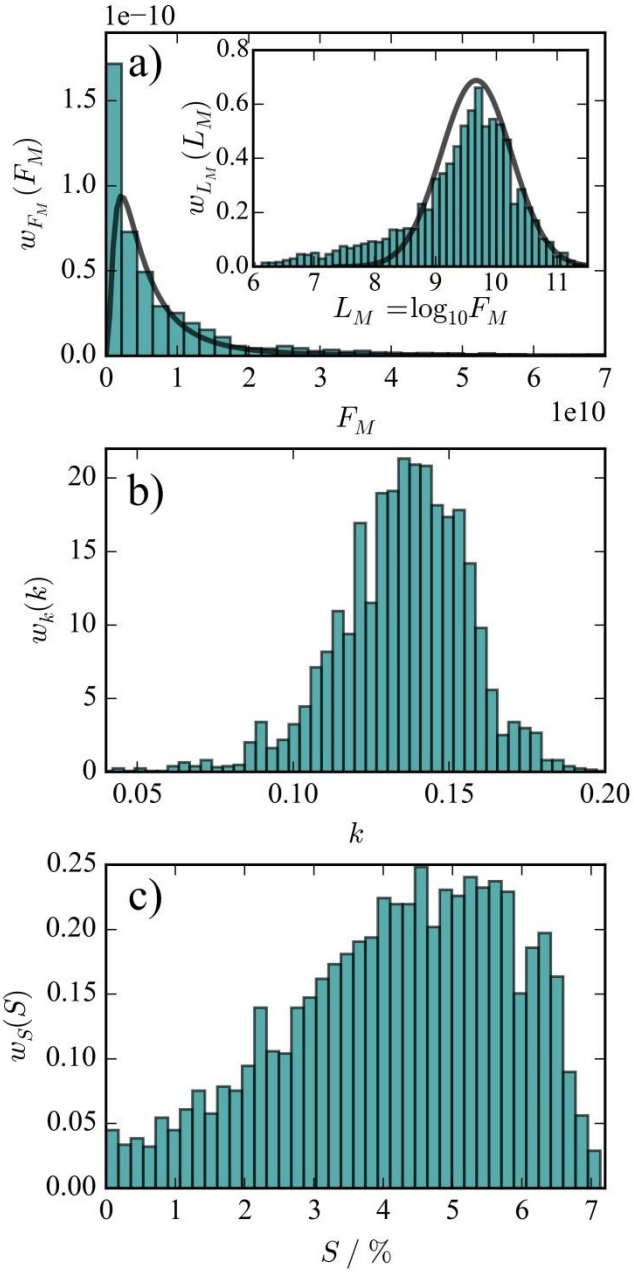

Figure S4: Normalized histograms of the simulated substrate HS parameters. a) The distribution of $\boldsymbol{F_M}$ is extremely skewed and broad (mean $\mathbf{1.06 \times 10^{10}}$, standard deviation $\mathbf{2.33 \times 10^{10}}$). To better resolve the distribution of enhancements, the distribution of $\boldsymbol{L_M = log_{10} F_M}$ is shown in the inset of a). Since it is approximately normally distributed (mean 9.39, standard deviation 0.95), $\boldsymbol{F_M}$ is correspondingly log-normally distributed. The black line in the main figure of a) is the result of application of Eq. S6, whose parameters have been determined by the least-squares fit results shown in Table 1 (main text of the manuscript); the black line in the inset of a) is the normal distribution of $\boldsymbol{L_M}$, with the same parameters.

$w_{F_M}(F_M)$ (Figure S4a) is an extremely rapidly decaying asymmetric distribution peaked

near HS strengths close to the lower-bound instrumental detection limit. High HS strengths are exceedingly scarcer than low HS strengths, as expected from the $g(F)$ curves of Figure S3. Therefore, to better resolve high enhancements, $L_M = log_{10}F_M$ is plotted in the inset of Figure S4a. In this representation, it is clear that F_M values range over 6 orders of magnitude, even though the geometrical parameters R and g for each HS are minimally perturbed from the mean values. This variation is caused by the sensitive structure-activity relationships in HSs, which are already are well studied [5,6], however this is the first time it has been shown that nanostructural perturbations in a collection of otherwise identical HSs lead to highly asymmetric HS strength distributions in which low strengths are exceedingly more probable than high strengths. This highlights the challenges of fabricating highly efficient substrates that contain HSs bearing identical SERS activity. The simulation indicates that not even order of magnitude precision in HS strength uniformity can be easily achieved experimentally.

k and S (Figure S4b and c) vary much less significantly. The smallest variation is found in k, with a standard deviation of 0.021 compared to the mean value of 0.135. Since the slope of a power-law expressed in log-log form (L vs. $log_{10}g(L)$) is $-k$, this corresponds to just a $\pm$16% standard deviation in the slope. S shows a larger variation, from $0 - 7\%$ of the total surface area for a dimer with $R = \mu_R$ and surface area $2 \times 4\pi{\mu_R}^2$. In rare instances when $S = 0$, the HS strength did not exceed the detection limit.

We therefore hypothesize that deviation of $g(F)$ from power-law behavior is dominantly caused by variation in F_M, rather than S and k. To test this hypothesis, we recalculated $g(F)$ for the substrate via Eq. S2, this time assuming each HS has $S = \overline{S}$ and $k = \overline{k}$ (blue x's in Figure S3). ($S = \overline{S}$ implies that a molecule is equally likely to adsorb to any HS and $k = \overline{k}$ implies each HS has the same scaling parameter). The overall convergence to the original curve makes it clear

that $g(F)$'s deviation from power-law behavior is the result of massive variation in F_M. It also illustrates that S and k are well modeled by their mean values, *i.e.* treating S and k as constant parameters. Therefore, $w_S(S)$ and $w_k(k)$ can be described by Dirac delta functions centered about their mean values:

$$w_S(S) = \delta\left(S - \overline{S}\right) \tag{S5}$$

$$w_k(k) = \delta\left(k - \overline{k}\right) \tag{S6}$$

Since variation in F_M occurs over 6 orders of magnitude, logarithmic measures of the distribution are more descriptive than their linear counterparts, and so we consider the form of $L_M = log_{10}F_M$ (Figure S4a). Except for a slight asymmetry observed in its tails, the bell-shaped nature of the distribution implies L_M can be modeled by a normal distribution. F is then correspondingly log-normally distributed:

$$w_{F_M}\left(F_M; \overline{L_M}, \sigma_{L_M}\right) = \frac{log_{10}\mathrm{e}}{F_M\sqrt{2\pi\sigma_{L_M}^2}}\exp - \left(\left(log_{10}F_M - \overline{L_M}\right)^2/2\,\sigma_{L_M}^2\right), \tag{S7}$$

where $\overline{L_M}$ and σ_{L_M} are the mean and standard deviation of $L_M = log_{10}F_M$. $\overline{L_M}$ and σ_{L_M} are related to the mean and standard deviation of F_M ($\overline{F_M}$ and σ_{F_M}) according to

$$\overline{F_M} = 10^{\overline{L_M} + \frac{1}{2}\sigma_{L_M}^2/log_{10}\mathrm{e}} \tag{S8}$$

$$\sigma_{F_M} = \overline{F_M}\sqrt{10^{\sigma_{L_M}^2/log_{10}\mathrm{e}} - 1}. \tag{S9}$$

We also modeled $\overline{F_M}$ with an exponential curve, however it grossly underestimated the distribution at high HS strengths.

In the approximation that S and k are constant, all three variables are statistically independent of one another, which implies $w(S,k,F_M)$ is the product of the three marginal distributions (Eqs. S5, S6, and S7):

$$w(S,k,F_M) = \delta\left(S-\overline{S}\right)\delta\left(k-\overline{k}\right)w_{F_M}\left(F_M;\overline{L_M},\sigma_{L_M}\right). \tag{S10}$$

Parameterized multi-HS model

Plugging Eq. S10 into Eq. S4 and solving the integrals with respect to S and k yields a parameterized form of the model:

$$g\left(F;\overline{L_M},\overline{k},\sigma_{L_M}\right) = \int_0^\infty w_{F_M}\left(F_M;\overline{L_M},\sigma_{L_M}\right)p\left(F;\overline{k},F_M\right)\,\mathrm{d}F_M\,, \tag{S11}$$

where $p\left(F;\overline{k},F_M\right)$ is given by Eq. S1 and $w_{F_M}\left(F_M;\overline{L_M},\sigma_{L_M}\right)$ is given by Eq. S7. Eq. S11 has 3 fitting parameters $\overline{L_M}$, σ_{L_M}, and $\overline{k}$, which together provide substantial information about a substrate:

- $\overline{L_M}$ (related to $\overline{F_M}$ by Eq. S8) is a measure of the average HS strength, an important measure for substrate efficiency. Commonly, the maximum HS strength for a substrate is determined by calculating F for the maximum intensity reading observed in a dataset of SERS measurements. However, doing so characterizes only the strongest HS in the substrate and says nothing about the strengths of all other HSs. Given how broad the distribution of F_M is, $\overline{L_M}$ is a much more useful statistic for assessing substrate quality.
- σ_{L_M} (related to σ_{F_M} by Eq. S9) is a principal measure of HS variation within a substrate. When σ_{L_M} is large, there is more variation among HS strengths.
- $\overline{k}$ describes, on average, how fast the probability of detecting large F decays on the substrate. It is a very important measurement of the characterization of the HSs in a

substrate. The relationship between this parameter and HS localization is further discussed in the main manuscript.

The assumptions of the model are that:

1. Each HS is statistically independent of other HSs.
2. Molecules adsorb with equal probability on all surface sites (HSs or not).
3. The number of HSs in the cross-section of the irradiating laser must be large enough for a continuum approximation of Eq. S3 to be valid.
4. The weighting factor distribution $w(S, k, F_M)$ of the parameters S, k, and F_M is well modeled by Eq. S10.

The simulations carried out above suggest that such assumptions are likely to hold for a variety of experimental conditions. An example using a roughened Ag electrode, a well-studied SERS substrate, is presented in the main manuscript.

Validation of equation 5 (from the main text)

To validate Eq. 5, by considering a single HS from the simulated substrate with $k = 0.12$ and using a cutoff of $F_{cutoff} = 1x10^8$, we obtained the SM-SERS intensity distribution in Figure S5. The estimated D' (Eq. 5 from the main text) is 5.8, which is very close to the D' from Eq. 4 ($D' = 6$). The observed difference is due to slight divergences in the simulated substrate from TPD-behavior as well as finite statistical sampling.

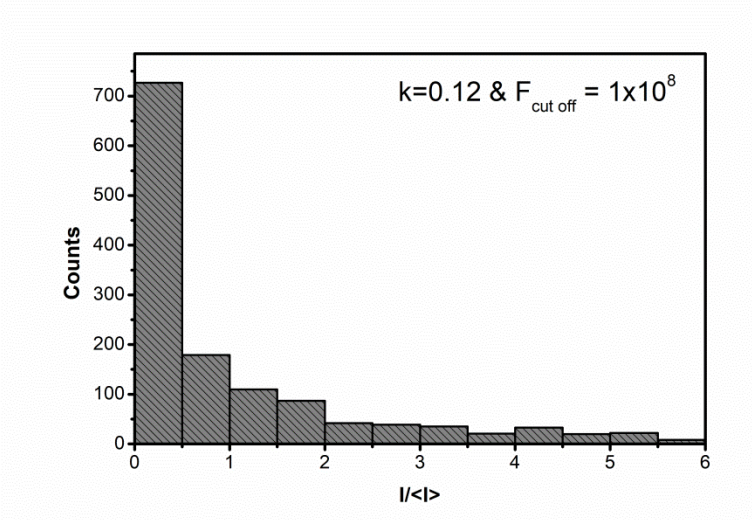

Figure S5: Simulated SM-SERS intensity distribution for a single HS with $k = 0.12$, after the introduction of a $F_{cutoff} = 1x10^8$, which simulates the instrumental detection limit of F.

Evaluating SERS efficiency of single HSs from simulated structures of different geometries

The experimental determination of F_M can in principle be obtained if we know the Raman cross-section of the molecule and we are certain that F_M is solely due to a single-molecule.[7,8] In the main manuscript, we discussed the influence of multiple adsorbing molecules (Figure 2), where the results suggest that such assumption are only approximate in certain experimental conditions, even at very low molecule numbers per HS.

k and D' can be directly obtained within our model from the SM-SERS intensity distributions. These two parameters (k and D') are related to the HS structure and its local field properties and therefore can be used to experimentally obtain fundamental information about the structure-activity relationship of the HSs in a given sample. This can be better visualized in Figure S6.

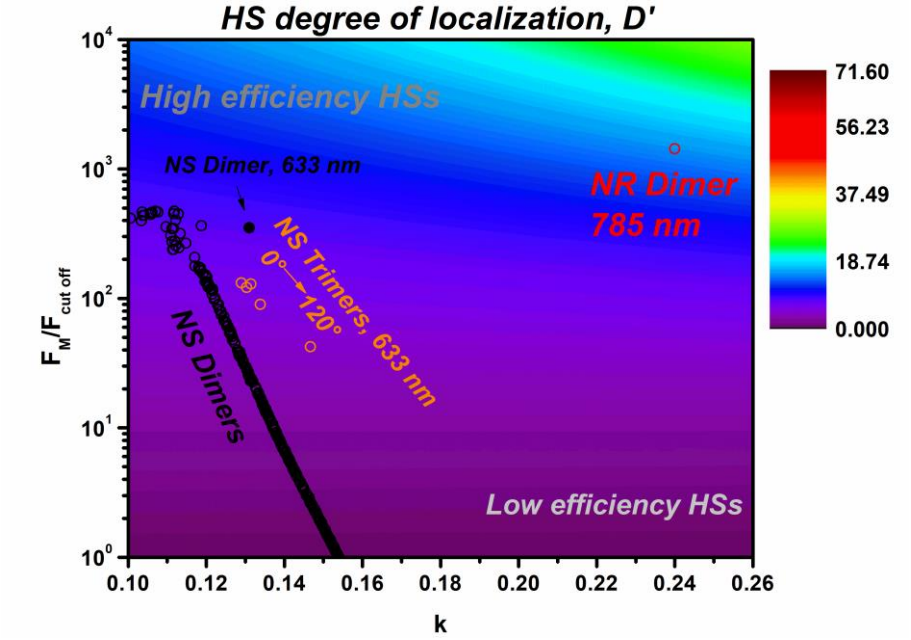

Figure S6: Map of D' as function of k and F_M/F_{cutoff} as calculated by Eq. 4 (main text). Also presented is the calculated k and F_M/F_{cutoff} for HSs in different structures, such as for silver nanospheres dimers (black solid and empty circles), trimers (orange circles) and gold nanorods (red circles).

Figure S6 presents a map of D' as a function of k and F_M/F_{cutoff}. Included in the figure are the k and F_M/F_{cutoff} parameters calculated for some of the nanosphere (NS) dimers in the simulated substrate used in the development of the model, which are presented as empty black circles. It can be seen that, at the conditions of the simulations (448 nm excitation and air as surrounding medium), F_M decreases with k. This is expected since k measures the probability of observing large F's from the distribution; as F_M decreases it becomes less probable to obtain large F's.

Since experimental SERS measurements are usually performed with nanoparticles in water as a dielectric environment, laser excitations at 633 nm and 785 nm, and at varying degrees of aggregation, we performed the simulations of a NS dimer (25 nm radii and gap 1nm, solid black circle in Figure S6), NS trimers (same radii and gap) and a gold nanorod (NR) (aspect ratio 3, length 45 nm and gap 1 nm) dimer for comparison of the effect of changing the nanoparticle

geometry. The gold NR geometry was chosen for comparison due to its large applicability in SERS studies.[9-12] The results for D', k and F_M/F_{cutoff} for all these structures are also presented in Figure S6. In the case of NS trimers and NR dimers, the procedure for constructing the $p(F)$ functions was not the same as in the case of NS dimers. In those systems, full 3D calculations of F on homogeneously distributed points on the surface of all nanoparticles forming a HS were performed, as it can be seen in Figure S7. The $p(F)$ function was then obtained from the histogram of such surface distribution of F values.

If we compare the results for different nanoparticle geometries (NS vs NR), we can clearly see that the NR dimer presents larger values of k and D', indicative of a HS with a highly localized field enhancement. This is an expected result since the NR geometry leads to strong field localizations due to the presence of tips, as it can be clearly seen in the surface distribution of F as calculated by DDA (Figure S7A).

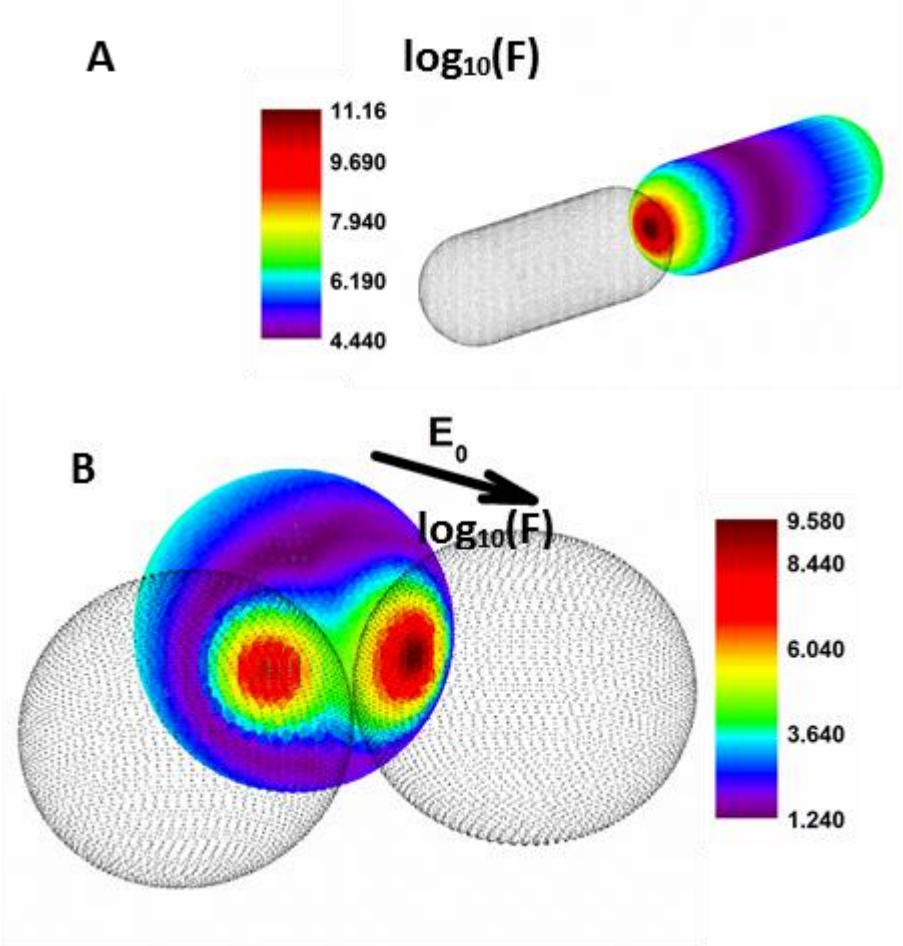

Figure S7: Results for F on the surface of a dimer of gold NRs (A) and a trimer of silver NSs (B), composed of equal nearly touching NSs (gap 1 nm).

In the case of aggregates of identical nanoparticle geometries (NS dimers vs NS trimers), trimer structures present larger k but smaller D' values as compared to the dimer, which is a result of the presence of interacting HSs in the trimers, as can be visualized from the F distribution on the surface of one of the particles in the structure (Figure S7B). Such interaction leads to a larger area of high F values (smaller D') and a faster decrease of the F distribution for each HS. These two interpretations about HS structure and properties can be readily obtained from electromagnetic simulations for simple structures such as the ones used in these examples. For a complex substrate these simulations are unfeasible, however this information can be

obtained by experimental determination of k and D' for the substrate. As an example, for the roughened electrode, the fit yielded $D' = 8.97$ and $k = 0.11$, which means that, on average, the HSs have properties that are closer to the simulated nanospheres than for structures with tips.

The above results suggest that k and D' can be used as a powerful tool for the characterization of complex electromagnetic interactions among HSs in various structures, which could be useful for studying electromagnetic interferences in plasmonic nanostructures. The above results also demonstrate that k and D' can be estimated from the experimental SM-SERS distribution.

The effect of substrate roughness

Finally, we apply the analysis developed so far to extract a deeper visualization of the properties of the roughened electrode substrate. An important question that can be raised in a system such as this is: what is the effect of electrode roughness on the HS parameters? In the oxidation and reduction activation cycles a variety of nanostructure sizes and shapes can be formed on the roughened electrode. In any two separated experiments, slight differences in applied potential, current density or electrolyte solution concentrations may lead to distinct distributions of nanostructures in terms of width and average size. This suggests that such characteristics (structure size variability and average size distribution) may have important effects on the substrate efficiency. Also, experiments may be performed with different light excitation wavelengths, which may or not be in resonance with the average HS structure. All such characteristics are analyzed in this section.

We start by analyzing the effect of distribution uniformity on the substrate properties by fixing the excitation wavelength and average nanostructure sizes. In the main text $\overline{L_M}$, σ_{L_M}, and $\overline{k}$ were calculated for a simulated substrate of 3500 HSs. To model the effect HS variability due to

the roughening procedure, we selected several subsets of the 3500 homodimers. Each one of those subsets defined distinct degrees of geometric heterogeneity. Specifically, we selected dimers that had radii within $\pm x$nm of the mean geometry ($R_x$nm), where x varied from ∞ to 1nm. Since increasing x corresponds to an increase in geometric heterogeneity, we use x as a proxy for roughness. Recalculating $\overline{L_M}$, σ_{L_M}, and $\overline{k}$ for each of the subsets yields the following table:

TABLE S1. Effect of the roughness of the distribution parameters.

x (nm)	R_x (nm)	$\overline{L_M}$	σ_{L_M},	k	D'
∞	5.03	9.4	0.95	0.1352	3.494
10	4.38	9.47	0.87	0.1350	3.711
9	4.15	9.5	0.85	0.1350	3.806
8	3.89	9.53	0.82	0.135	3.902
7	3.54	9.59	0.78	0.1348	4.095
6	3.17	9.64	0.75	0.1349	4.260
5	2.71	9.7	0.7	0.1347	4.460
4	2.2	9.77	0.64	0.1348	4.699
3	1.7	9.84	0.59	0.1345	4.942

2	1.17	9.88	0.55	0.1346	5.084
1	0.58	9.91	0.5	0.1343	5.190

As x decreases and the substrate becomes less geometrically heterogeneous (indicated by a decrease in R_x), a larger maximum SERS enhancements can be observed (as indicated by the values of $\overline{L_{\mathrm{M}}}$) with a smaller variability in the maximum enhancement (σ_{L_M} decreases). Note that the increase in $\overline{L_{\mathrm{M}}}$ is only a result of the fact that the excitation wavelength is, by design, optimized for the mean geometry. The above result is in accordance with the expected: as we increase the number of HSs with resonances shifted from the excitation wavelength (large x), the total enhancement will decrease. The k parameter shows a much smaller variation than $\overline{L_{\mathrm{M}}}$ and D', which is a result that in such simulations, the average sizes of the nanoparticles were the same (only the width of the distribution was changed), and since k is an average property of the distribution, it is expected that the variability in such a parameter to be small. It can be observed though a small increase in k as the HS distribution becomes broader (large x), due to a lower efficiency for the HSs to generate large enhancements, in accordance to the data for NS dimers and trimers of Figure S6.

To probe the effect of excitation wavelength, we analyzed two HS distributions (substrate 1 and substrate 2) in water environment. This approach was taken with the objective to better correlate the results with experiments, whose conditions usually take as excitation wavelengths 633 nm (as in the case of the electrode substrate in this paper) and 785 nm. Hence, the observation of large enhancements (for SM-SERS detection) for such radiations requires the

homodimers to be in water environment or a medium with larger refractive index. Figure S8 shows a map for L_M for different combinations of nanoparticle radius and gap sizes for two excitation wavelengths: 633 nm (A) and 785 nm (B). Also in Figure S8 it is also shown the geometric parameter distributions that characterize substrates 1 and 2. The contour lines in the map of L_M are presented in each figure and span the interval 4 (dark blue) to 12 (dark red).

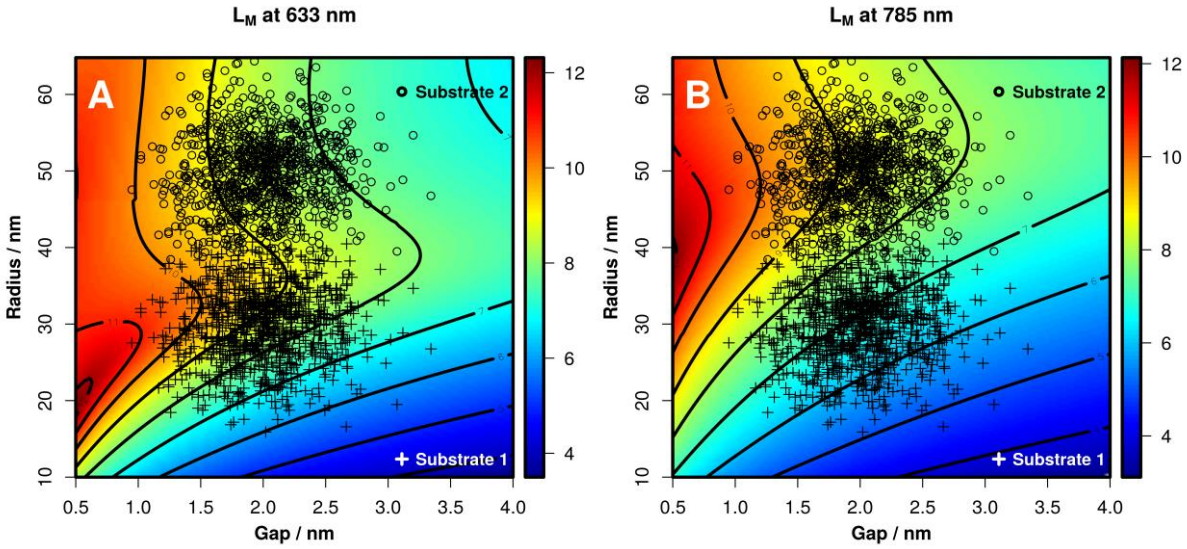

Figure S8: Map of L_M for different combinations of radius and gap sizes for Ag homodimers in water environment. The maps were obtained for 633 nm (A) and 785 nm (B) excitations. The crosses and circles represent the distributions of radius and gaps that characterize the two substrates: substrate 1 and substrate 2, respectively.

From Figure S8 it is possible to observe very distinct behavior from the two simulated substrates for each exciting radiation. For 633 nm, it can be observed a significant distribution of HSs in substrate 1 that present L_M > 9 as well as L_M < 8, which leads to a relatively low $\overline{L_M}$ and large σ_{L_M}, as it can be seen in Table S2. On the other hand, for this radiation, most of HSs in substrate 2 present L_M in the interval 8 to 9, giving to this substrate the characteristic of a larger $\overline{L_M}$ and lower σ_{L_M}. The D' parameter takes into account k, and for the larger D' value observed

for substrate 1 (relative to substrate 2) suggests a higher degree of HS localization (Table S2). This is in agreement to the substrates characteristics depicted in Figure S9; i.e., the 633 nm excitation is closer to the resonance condition for substrate 1, relative to substrate 2.

TABLE S2. Parameters for substrate 1 and 2 of Figure S8 for excitation at 633 nm and 785 nm.

System	$\overline{L_M}$	σ_{L_M}	k	D'
Substrate 1 (633 nm)	7.76	1.097	0.123	8.38
Substrate 1 (785 nm)	6.27	0.732	0.155	2.30
Substrate 2 (633 nm)	8.60	0.431	0.101	4.97
Substrate 2 (785 nm)	8.69	0.483	0.121	7.85

Similarly, a larger degree of localization is observed for substrate 2 at 785 nm excitation (larger *D'* value), as expected, once larger particles present resonances closer to 785 nm radiation wavelength (see Fig. S9).

An interesting aspect of Table S2 is related to the k-values. For substrate 1, it can be observed an increase in k from 633 nm to 785 nm, which is associated to the decrease in the average enhancement, since 785 nm wavelength is away from resonances (Figure S9). This is in accordance to the results of Table S1. The same trend can be observed if the radiation wavelength is fixed. For instance at 785 nm, the observed k is smaller for substrate 2 then substrate 1, which is in accordance to the fact that the former present HSs with resonances that are closer to this excitation wavelength.

An exception to the above analysis is substrate 2 excited with 633 nm, which presented the smallest k value, even though the system is not in resonance with the excitation radiation, as it can be seen in Figure S9. For a better understanding of such result, Figure S10 shows the map of L_M for a homodimer that mimics the average HS in substrate 2.

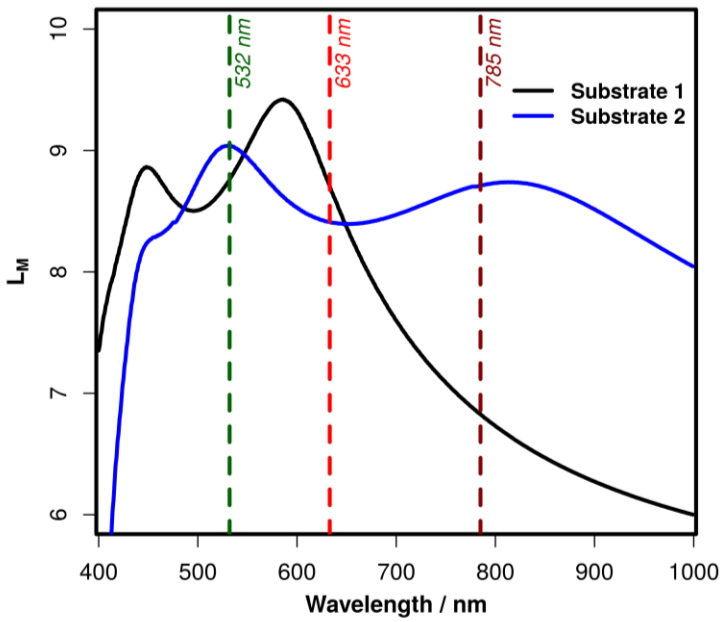

Figure S9: Simulation of L_M as function of wavelength for the average HSs of Figure S8 that characterize substrates 1 and 2. The vertical dashed lines represent excitation wavelengths.

The L_M map of Figure S9 shows an enhancement distribution shape that presents a contribution from a higher order plasmon mode, whose resonance wavelength is observed at 532 nm excitation wavelength.

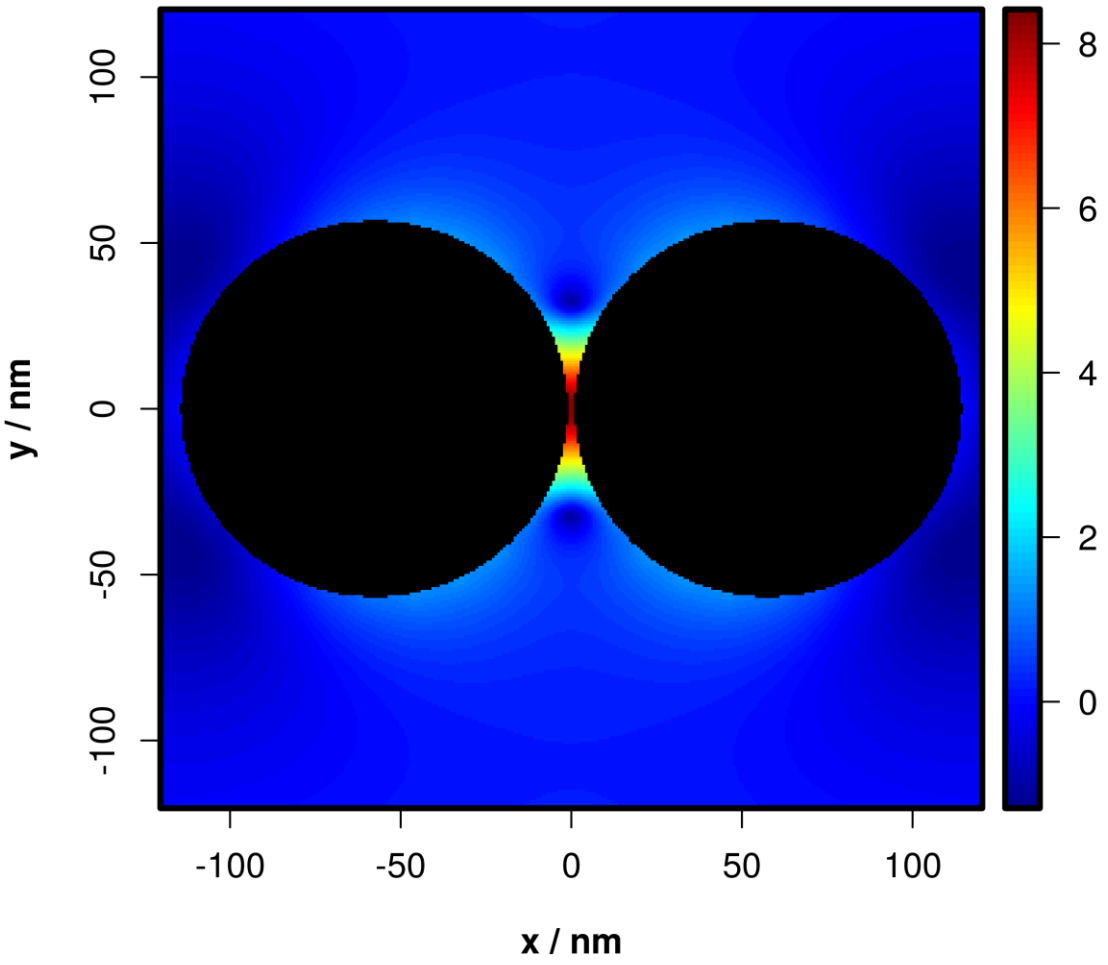
y / nm
100
50
0
-50
-100
-100
-50
0
50
100
x / nm
8
6
4
2
0

Figure S10: Map of L_M for a homodimer that describes the average HS in substrate 2. Excitation at 633 nm.

The L_M spectra in Figure S9 show that for 785 nm excitation the HS is formed by a dipolar coupling between dipole plasmon modes, whereas at 532 nm the HS is formed by a coupling involving higher order plasmon modes. Therefore, we should expect that the HS at 633 nm presents a hybrid characteristic between these two limits. We hypothesize that the smaller k observed at 633 nm may be related to the contribution of higher order plasmon modes in the enhancement factor distribution. If this statement is correct, we should be able to observe an even smaller value of k for 532 nm excitation. The simulation at such wavelength yielded k approximately equal to 0.06 and D' approximately equal to 1.9, showing that the contribution of higher order modes contributes to diminishing k, without increasing D'.. Therefore, k and D' can also be used to infer about the structure of the roughened electrode substrate in terms of the size distribution.

The roughened silver electrode in the main text yielded for 633 nm values for k and D' 0.11 and 8.97, respectively. The magnitude of k and D' measured in the experiment is close to the simulated substrate 1 at the same radiation. This suggest that the distribution of sizes in substrate 1 can be used as a proxy for the description of the electrode particle size distribution, which is in accordance to our expectation from the stochastic process of generating nanostructures by the electrochemical method. We should expect from this procedure a very broad distribution of enhancement factors in the same way as substrate 1 in Figure S8.

References

(1) Burroughs, S. M.; Tebbens, S. F. *Fractals* **2001**, *9* (2), 209–222.

(2) Le Ru, E. C.; Etchegoin, P. G.; Meyer, M. *J. Chem. Phys.* **2006**, *125* (20).

(3) Le Ru, E. C.; Etchegoin, P. G. *Chem. Phys. Lett.* **2006**, *423* (1–3), 63–66.

(4) Wang, Z. B.; Luk'yanchuk, B. S.; Guo, W.; Edwardson, S. P.; Whitehead, D. J.; Li, L.; Liu, Z.; Watkins, K. G. *J. Chem. Phys.* **2008**, *128* (9).

(5) Kleinman, S. L.; Sharma, B.; Blaber, M. G.; Henry, A.-I.; Valley, N.; Freeman, R. G.; Natan, M. J.; Schatz, G. C.; Van Duyne, R. P. *J. Am. Chem. Soc.* **2013**, *135* (1), 301–308.

(6) Henry, A.-I.; Wustholz, K. L.; Tyler, T. P.; Alexander, K. D.; Lopez, R.; Freeman, R. G.; Natan, M. J.; Schatz, G. C.; Hersam, M. C.; Van Duyne, R. P. *Abstr. Pap. Am. Chem. Soc.* **2011**, *242*.

(7) Le Ru, E. C.; Blackie, E.; Meyer, M.; Etchegoin, P. G. *J. Phys. Chem. C* **2007**, *111* (37), 13794–13803.

(8) Etchegoin, P. G.; Lacharmoise, P. D.; Le Ru, E. C. *Anal. Chem.* **2009**, *81* (2), 682–688.

(9) Lee, A.; Andrade, G. F. S.; Ahmed, A.; Souza, M. L.; Coombs, N.; Tumarkin, E.; Liu, K.; Gordon, R.; Brolo, A. G.; Kumacheva, E. *J. Am. Chem. Soc.* **2011**, *133* (19), 7563–7570.

(10) Blaber, M. G.; Schatz, G. C. *Abstr. Pap. Am. Chem. Soc.* **2011**, *242*.

(11) Lee, A.; Ahmed, A.; dos Santos, D. P.; Coombs, N.; Park, J. Il; Gordon, R.; Brolo, A. G.; Kumacheva, E. *J. Phys. Chem. C* **2012**, *116* (9), 5538–5545.

(12) Lin, K.-Q.; Yi, J.; Hu, S.; Liu, B.-J.; Liu, J.-Y.; Wang, X.; Ren, B. *J. Phys. Chem. C* **2016**, *120* (37), 20806–20813.